



Article

# Porcelain Ceramic Tile Manufactured with the Addition of Hydroxyapatite in Ceramic Formulations

Flávio Pessoa Avelino <sup>1,2</sup>, Wendel Melo Prudêncio de Araujo <sup>1</sup>, Roberto Arruda Lima Soares <sup>1</sup>,  
Ramon Peña-García <sup>3</sup>  and Anderson O. Lobo <sup>2,\*</sup> 

<sup>1</sup> Materials Science and Engineering Graduate Program, Interdisciplinary Laboratory for Advanced Materials, Federal University of Piauí, Teresina 64049-550, PI, Brazil; flaviop.avelino@ifpi.edu.br (F.P.A.); wendelprudencio@hotmail.com (W.M.P.d.A.); robertoarruda@ifpi.edu.br (R.A.L.S.)

<sup>2</sup> Postgraduate Program in Materials Engineering PPGEM, IFPI Campus, Teresina 64000-040, PI, Brazil

<sup>3</sup> Graduate Program in Engineering Physics, Academic Unit of Cabo de Santo Agostinho, Federal Rural University of Pernambuco, Cabo de Santo Agostinho 52171-900, PE, Brazil; ramon.raudel@ufrpe.br

\* Correspondence: lobo@ufpi.edu.br

**Abstract:** In this study, we developed formulations of a clay, kaolin, quartz, talc, and feldspar ceramic coating as a standard formulation, with the addition of Hap to improve the mechanical characteristics of the final product. The addition of Hap will help to fill the gaps in the formulation. Furthermore, it could lower the sintering temperature due to the high presence of calcium oxide in its composition. The main mineralogical phases (mullite, quartz, and anorthite) were identified in the sintered samples by X-ray diffraction. After evaluating the physical–mechanical properties (water absorption, linear shrinkage, apparent porosity, and resistance to flexion), the incorporation of Hap (5% in weight, 10% in weight, and 20% in weight) significantly altered the physical and mechanical properties of the final product, where we obtained, in relation to the standard formulation, an increase of more than 15% in mechanical resistance.

**Keywords:** Hap; ceramic formulations; sustainable materials



**Citation:** Avelino, F.P.; de Araujo, W.M.P.; Lima Soares, R.A.; Peña-García, R.; Lobo, A.O. Porcelain Ceramic Tile Manufactured with the Addition of Hydroxyapatite in Ceramic Formulations. *Minerals* **2023**, *13*, 1120. <https://doi.org/10.3390/min13091120>

Academic Editor: Alberto De Bonis

Received: 30 May 2023

Revised: 21 July 2023

Accepted: 23 July 2023

Published: 25 August 2023



**Copyright:** © 2023 by the authors. Licensee MDPI, Basel, Switzerland. This article is an open access article distributed under the terms and conditions of the Creative Commons Attribution (CC BY) license (<https://creativecommons.org/licenses/by/4.0/>).

## 1. Introduction

Ceramic coatings are materials composed of clay and other inorganic elements, which undergo processes, such as pressing and firing at high temperatures. They are used to coat floors and walls both indoors and outdoors in civil construction [1]. The ceramic tile industry worldwide depends on raw materials, mainly clays, to produce its products. Some regions may have an abundance of certain types of clay, while others are scarce. The ceramic tile industry faces challenges regarding the economy of quality raw materials in some regions, which affects the production and prices of ceramic materials. To overcome these challenges, the industry can invest in research that includes synthetic raw materials, such as zirconium, alumina, and silica. The use of synthetic raw materials can provide benefits related to the quality and stability of ceramic products, in addition to reducing dependence on natural raw materials and increasing the sustainability of the industry [1,2]. Estimates show that these activities produce more than 20 billion tons of solid waste annually. Over half is disposed of inappropriately with little or no responsibility [3–7]. The development of new alternative raw materials has attracted the attention of many researchers interested in reducing the environmental impact caused by these residues [8–11]. A viable and interesting alternative for ceramic tile formulations is the incorporation of synthetic hydroxyapatite (Hap) due to its excellent mechanical and physical–chemical properties, as it has low mass, high surface area, and excellent thermal stability, allowing its use at high temperatures during the coating firing process.

The high hardness and mechanical resistance of Hap improve the durability and resistance to abrasion of the coating. Its high concentration of calcium oxide can help to

reduce the firing temperature of the compound formed. In addition, HAP is a biodegradable material [12–14].

Porcelain tile stands out among ceramic tiles produced worldwide due to its technical properties and aesthetics. The worldwide demand for this ceramic coating grows daily, prompting industry and research centers to seek alternatives to traditional raw materials [15–17]. In general, the masses for porcelain tiles contain a high content of melting/refractory clays and feldspar, which are rich in melting oxides, such as calcium, potassium, sodium, and magnesium. This mass is fired in industrial kilns at very high temperatures of approximately 1200 °C with firing cycles of around 60 min, transforming it into ceramic materials with crystalline phases, for example, mullite, whose formation is due to the fusion of silicon oxides with aluminum oxides [18–20]. The main requirements for porcelain tiles are a high degree of whiteness, high density, low apparent porosity, high mechanical resistance, and deficient water absorption. Achieving these objectives leads to an adequate microstructure in the fired coating. The microstructure formed must be characterized by the complete or partial absence of apparent porosity [20–22]. Among several transformations during the firing process, the densification of the coating occurs due to a sintering mechanism through a viscous liquid phase caused by a large number of melting agents in the composition (feldspar and melting clays) [22,23]. In this procedure, the liquid phase plays an essential role in determining the densification of the ceramic piece [23,24].

Given the abovementioned factors, the main objective of this work is to evaluate the potential of adding Hap in proportions of 5 wt%, 10 wt%, and 20 wt% in the formulation to result in technical specifications that meet international standards, thus, enabling the production of an alternative porcelain tile ceramic covering. Currently, the scientific literature does not include an investigation about the incorporation of hydroxyapatite (Hap) into ceramic coating formulations [25]. Therefore, a study dedicated to examining this possibility would be of great importance to academia.

## 2. Materials and Methods

### 2.1. Raw Material

The clay, kaolin, feldspar, and quartz were purchased from Risi Produtos Cerâmicos in Cunha, State of São Paulo, Brazil. Talc was collected from mineral deposits in Dirceu Arcoverde in Piauí, Brazil. Hap was obtained from Graphen Tecnologia.

The raw materials used in this study are presented in Table 1.

**Table 1.** Origins of raw materials used to conduct this work.

Material	Feature
Feldspar *	Containing essentially the phases: microcline—(K, Na)AlSi <sub>3</sub> O <sub>8</sub> and albite—Na(AlSi <sub>3</sub> O <sub>8</sub> )
Light burning clay *	Containing essentially the phases: silicon oxide—SiO <sub>2</sub> and kaolinite—Al <sub>2</sub> (Si <sub>2</sub> O <sub>5</sub> )(OH) <sub>4</sub>
Kaolin *	Containing essentially the phases: kaolinite—Al <sub>2</sub> (Si <sub>2</sub> O <sub>5</sub> )(OH) <sub>4</sub> and microcline—K(AlSi <sub>3</sub> O <sub>8</sub> )
Quartz *	Containing essentially the phase: silicon oxide—(Si <sub>2</sub> )
Talc **	Containing essentially the phases: dolomite—CaMg(C <sub>3</sub> ) <sub>2</sub> and talc—Mg <sub>3</sub> Si <sub>4</sub> O <sub>10</sub> (OH) <sub>2</sub>
Hydroxyapatite ***	Essentially containing the phase: hydroxyapatite—Ca <sub>5</sub> (PO <sub>4</sub> ) <sub>3</sub> (OH)

Origins: \* Risi Ceramic Products; \*\* Dirceu Arcoverde—Piauí; \*\*\* Federal University of Piauí.

The materials were dried until they reached their maximum capacity to absorb moisture from the air under equilibrium conditions (hygroscopic humidity), and were then ground in a ball mill for 48 h and passed through an N° 44 µm sieve. The raw materials

were characterized in crystalline phases by X-ray diffraction (XRD) through particle size distribution and chemical analysis using the X-ray fluorescence (XRF) technique.

The chemical composition of the raw materials was measured using X-ray fluorescence (Shimadzu, model EDX 720, Kyoto, Japan). The mineralogical phases of the raw materials and sintered samples were identified by X-ray diffraction (Shimadzu XRD 6000 model, Kyoto, Japan), with the X-ray wavelength (Cu = 40 Kv/30 mA) and range of  $2\theta$  from  $10^\circ$  to  $70^\circ$ , in accordance with the JCPDS database. Particle size distribution was determined by laser diffraction (Cilas, model 1064LD, Orléans, France). The thermal behaviors were evaluated by thermogravimetry (TG)/derived thermogravimetry (DTG) (DTG Shimadzu, model TA 60H, Kyoto, Japan), with a heating rate of  $5^\circ\text{C}/\text{min}$ , under a nitrogen gas atmosphere as standard.

## 2.2. Sample Preparation

The compositions were formulated based on a standard composition (45 wt% feldspar, 30 wt% clay, 15 wt% kaolin, 7 wt% quartz, and 3 wt% talc), in which 5 wt%, 10 wt%, or 20 wt% of Hap were added to improve the technical characteristics of the final product. The nominal compositions of the ceramic formulations (wt%) and their respective nomenclatures are summarized in Tables 2 and 3. The default composition was based on the literature [26].

**Table 2.** Nomenclature and nominal composition (wt%) of the standard formulation studied in this research.

Raw Material	Composition (wt%)
Feldspar	45
Clay	30
Kaolin	15
Quartz	7
Talc	3

**Table 3.** Nomenclature and nominal composition (wt%) of the standard formulation with the addition of Hap studied in this research.

Raw Material	Composition (wt%)		
Standard formulation	95	90	80
Hydroxyapatite (5%, 10%, and 20%)	5	10	20

The selected raw materials were calculated to provide 5.0 kg of standard composition material. The raw materials were homogenized wet in a ball mill (SOLAB ball mill) in a 1:1 ratio (one portion of water to one portion of composition) for 24 h. The samples were formed in a metallic prismatic matrix (10 mm  $\times$  10 mm  $\times$  80 mm). The samples were obtained from 18 to 20 g of powder in a hydraulic press at a pressure of  $750\text{ kg}/\text{cm}^2$ , with a force of around 6.0 tons applied for 30 s. Ten samples of each formulation were produced for each temperature. Quality control was performed by selecting the six best samples, considering the absence of small cracks, size, and conformation quality. After pressing and drying, the green densities for samples of all compositions ranged from  $1.80$  to  $2.00\text{ g}/\text{cm}^3$ . Notably, these values are below those usually used for forming porcelain tile compositions (around  $2.0$  to  $2.1\text{ g}/\text{cm}^3$ ) [26,27]. Finally, the pressed samples were dried at  $110^\circ\text{C}$  for 24 h and sintered in a conventional electric furnace.

## 2.3. Characterization Samples after Sintering Treatment

The sintering protocol consisted of a heating rate equal to  $5^\circ\text{C}/\text{min}$ , 30 min at the final temperatures of  $1000^\circ\text{C}$ ,  $1100^\circ\text{C}$ , and  $1200^\circ\text{C}$ , and natural cooling to room temperature.

The characterization of the powders of the burnt compositions was carried out, characterizing them in terms of crystalline phases by X-ray diffraction (DRX); this method

determines the crystalline structure of the sintered compositions. This analysis was used to determine the formation of crystalline phases and provide information about the crystalline structure of the samples. It is a fast and easy-to-use method that provides detailed information about the crystalline structure of sintered materials. Scanning electron microscopy was also used to verify the distribution of total open and closed porosity, the normal and fracture surface, and the morphology of the material. Scanning electron microscopy was then used to detect and map the porosity distribution in the material. The obtained data made it possible to determine the total porosity, pore dimensions, and other properties.

The fired samples were characterized using the Archimedes method to measure water absorption and apparent porosity. Flexural strength measurement was performed using the three-point flexion test. The procedures for carrying out these tests are all supported by standards [28–34].

### 2.3.1. Linear Retraction (LR)

Linear shrinkage considers the variation in the linear dimension of the ceramic body, in percentage, after the sintering step. A variation with a positive value characterizes a retraction of the dimension initially considered. Otherwise, it is considered that the ceramic body underwent expansion. The procedure adopted was the measurement with a caliper of the lengths of the specimens before and after sintering. The following equation was used to calculate the linear shrinkage values after firing:

$$LR(\%) = \frac{(L0 - Lf)}{Lf} 100\%$$

where  $LR$  is the linear shrinkage value, as a percentage, of the specimen after sintering;  $L0$  is the length of the specimen before sintering, and  $Lf$  is its length after the sintering process.

### 2.3.2. Water Absorption (WA)

Water absorption is the percentage value of the mass of water absorbed by the body after sintering. The water absorption test was carried out as follows: the specimens were weighed immediately after leaving the oven on an analytical balance. Consecutively, they were submerged in distilled water for 24 h in a glass container. After this time, they were removed from the container, and excess surface water was removed with a damp cloth and immediately weighed to verify the variation in their new masses. The water absorption value, in mass percentage, was obtained using the following equation below:

$$WA(\%) = \frac{Mu - Mq}{Mu} 100\%$$

where  $WA$  is the water absorption as a percentage;  $Mu$  is the mass of the specimen saturated in water;  $Mq$  is the mass of the dry sample. After calculating the water absorption of each sample, the arithmetic mean of the values obtained for each group was calculated.

### 2.3.3. Apparent Porosity (AP)

The calculation of the apparent porosity provides the probable percentage of the volume of open pores, after sintering, of the specimens concerning their total volume. Obtaining this value was calculated as follows: after weighing the specimens to calculate the water absorption, the mass of the immersed samples was also measured using the hydrostatic balance method. With the three values,  $Mu$ ,  $Mq$ , and immersed body mass  $Mi$ , the following equation was used to obtain the percentage value of the apparent porosity:

$$AP(\%) = \frac{(Mu - Mq)}{Mu - Mi} 100\%$$

where  $AP$  is the calculated value of the apparent porosity, and  $Mi$  is the mass of the specimen immersed in water.

### 2.3.4. Three-Point Bending Failure Stress (TRF)

Flexural rupture stress refers to the material's resistance to simple flexion by the three-point method, according to the method proposed by VICAT. To measure this property, a universal testing machine, model AG—I 250 KN, from Shimadzu, was used, operating at a speed of 0.5 mm/min, according to the method proposed by the standard (AMERICAN SOCIETY FOR TESTING AND MATERIALS) (ASTM). Tests were performed on six specimens for each formulation to obtain the results, and the arithmetic mean of these values gave the final value. The calculations were performed automatically by the Trapezium 1.14 software from Shimadzu. The following equation provides the results:

$$TRF \left( \text{kg/cm}^2 \right) = \frac{3pl}{bh^2} 100\%$$

where  $TRF$  is the breakdown tensile ( $\text{kg/cm}^2$ );  $p$  is the load reached at the moment of failure (kg);  $l$  is the distance between the supports of the specimen;  $b$  is the width of the sample;  $h$  is the height of the sample.

## 3. Results and Discussions

### 3.1. Characterization of Raw Materials

Figure 1a–f and Table 4 are the diffractograms and the chemical compositions of the raw materials. Figure 1a indicates that the clay used consisted of kaolinite  $\text{Al}_2(\text{Si}_2\text{O}_5)(\text{OH})_4$  (JCPDS: 78-2110) and quartz ( $\text{SiO}_2$ ) (JCPDS: 46-1045) phases, which provide plasticity to the mass and mechanical resistance to the final product [35–37]. Figure 1b shows kaolin, which will produce lighter-colored sintered parts. In addition, kaolinite is a fundamental carrier of aluminum oxide ( $\text{Al}_2\text{O}_3$ ) (JCPDS: 10-0173). During the vitrification phase, the ceramic mass becomes a regulator of the balance of reactions, resulting in the formation of mullite ( $3\text{Al}_2\text{O}_3 \cdot 2\text{SiO}_2$ ) (JCPDS: 79-1276), which, due to its structure, will function as “bone,” increasing its resistance [38,39]. The kaolin used as one of the raw materials for making the sintered samples consisted of the kaolinite phase  $\text{Al}_2(\text{Si}_2\text{O}_5)(\text{OH})_4$  (JCPDS: 78-2110). Figure 1c shows the feldspar, which can play a crucial role in porcelain tile ceramic masses due to these minerals, the high gresification, high mechanical resistance, and reduced porosity after firing [40,41]. The feldspar used consisted of the following phases: potassium feldspar— $(\text{K}, \text{Na})\text{AlSi}_3\text{O}_8$  (JCPDS 10-0357) and sodium feldspar— $\text{Na}(\text{AlSi}_3\text{O}_8)$  (JCPDS 10-0357). Figure 1d shows the quartz that can maintain a siliceous “skeleton” in the mass when the other components soften due to increased temperature [40–42]. Furthermore, quartz, an essential regulator between silica ( $\text{SiO}_2$ ) (JCPDS: 46-1045) and alumina ( $\text{Al}_2\text{O}_3$ ) (JCPDS: 10-0173), contributes to the formation of mullite ( $3\text{Al}_2\text{O}_3 \cdot 2\text{SiO}_2$ ) (JCPDS: 79-1276), a phase that increases the mechanical resistance of the product [42]. The quartz used consisted of the ( $\text{SiO}_2$ ) phase (JCPDS: 46-1045), with no evidence of impurities and/or clay minerals within the detection limits of the X-ray analysis. The talc in Figure 1e is considered as flux energy. Its presence increases the fusibility by forming a eutectic with feldspar, which produces a large amount of low-viscosity liquid phase, helping densification and reducing porosity [42,43]. The talc used consisted of the following phases: dolomite— $\text{CaMg}(\text{CO}_3)_2$  (JCPDS 05-0622) and talc— $(\text{Mg}_3\text{Si}_4\text{O}_{10})(\text{OH})_2$  (JCPDS 29-1493). Figure 1f shows the hydroxyapatite used as an alternative additive in the composition of porcelain tiles. As Hap is a material essentially rich in calcium, it is expected to help reduce the final firing temperature of the porcelain tile coating [25]. The Hap consisted of the following phases: Hap— $\text{Ca}_5(\text{PO}_4)_3(\text{OH})$  (JCPDS 09-0432). The XRF technique evidenced that the raw materials have a high degree of purity, as shown in Table 4. All raw materials have a low iron oxide content, which is a significant value for porcelain ceramic tiles, as the presence of this oxide causes the final product to lose its light color.

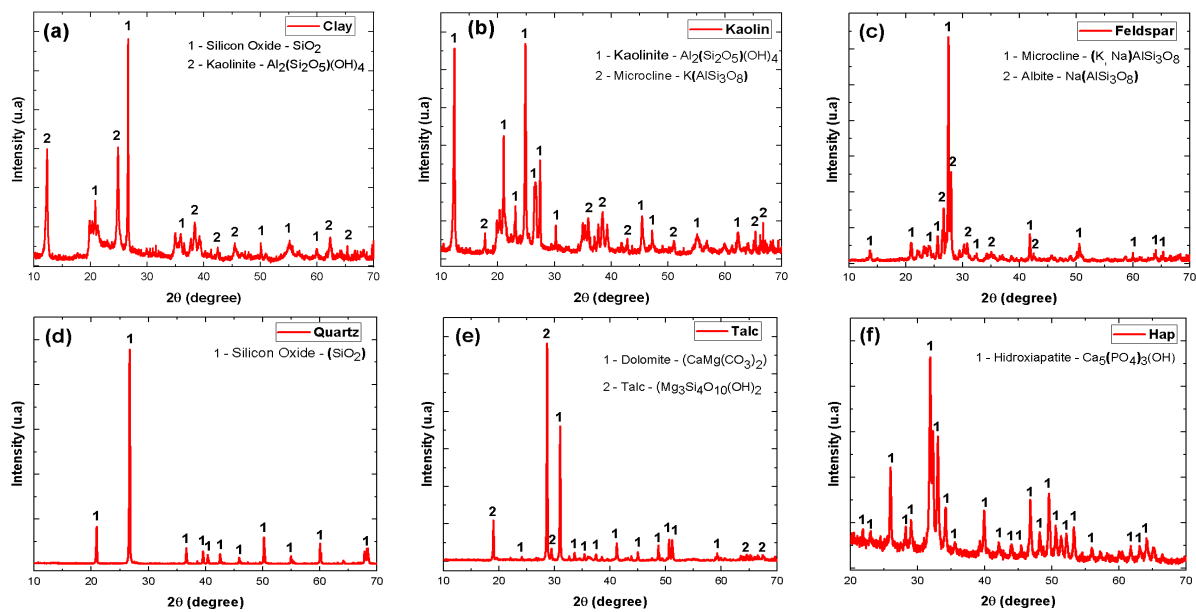


**Figure 1.** X-ray diffraction (XRD) patterns measured from clay (a), kaolin (b), feldspar (c), quartz (d), talc (e), and Hap (f).

**Table 4.** Chemical composition of the raw materials (clay, kaolin, quartz, talc, feldspar, and Hap) used in the new ceramic formulation studied.

Sample	SiO <sub>2</sub>	Al <sub>2</sub> O <sub>3</sub>	Fe <sub>2</sub> O <sub>3</sub>	CaO	Na <sub>2</sub> O	K <sub>2</sub> O	TiO <sub>2</sub>	MgO	P <sub>2</sub> O <sub>5</sub>
Clay	49.50	46.44	2.01	0.11	-	0.63	1.30	-	-
Kaolin	50.44	46.15	0.39	-	-	3.03	-	-	-
Quartz	99.88	-	-	-	-	0.12	-	-	-
Talc	39.55	-	1.15	22.06	-	-	-	37.13	-
Feldspar	65.06	20.57	0.11	-	5.80	8.41	-	-	-
Hydroxyapatite	-	0.20	-	62.41	-	-	-	0.42	36.74

Table 4 summarizes the chemical compositions of the raw materials (clay, kaolin, quartz, talc, feldspar, and Hap). The main oxides identified in the clay and kaolin were SiO<sub>2</sub> (49.50% and 50.44%) and Al<sub>2</sub>O<sub>3</sub> (46.44% and 46.15%), respectively. These oxides commonly originate from the structure of clay minerals and free silica [44,45]. Furthermore, a high K<sub>2</sub>O (3.03%) content was detected in kaolin. The presence of K<sub>2</sub>O is significant because it is a known flux and acts by decreasing the sintering temperature, providing economic benefits to the industry. Quartz contained SiO<sub>2</sub> (99.88%) as the main constituent, presenting excellent purity, indicating its potential as a flow agent and in forming “bones” in the finished ceramic coating. In addition, quartz helps to reduce the temperature maturation of the ceramic bodies, reducing energy consumption [46,47]. The high levels of CaO (22.06%) and MgO (37.13%) identified in the talc are associated with dolomite. CaO and MgO are essential to reduce refractoriness. However, a high fire loss can be attributed to the thermal decomposition of calcium carbonate and the release of gases. The greater amount of K<sub>2</sub>O (8.41%) and Na<sub>2</sub>O (5.80%) present in the feldspar contributes to the formation of the glassy phase during sintering, increasing the densification and ceramic resistance of the ceramic body and decreasing the porosity after firing [47]. Hydroxyapatite can reduce the refractoriness of the ceramic piece due to its high concentration of CaO (62.41%).

Figure 2a–f presents the particle sizes of each raw material used in the experiment. Their average values, D<sub>50</sub>, are in the order of 10 to 20 μm. The exception is talc particles, with a D<sub>50</sub> value of around 40 μm, above the recommended value for the coating production of porcelain ceramics of around 20 μm. However, the amount of talc in the mass is only 3 wt%, so talc should not significantly alter the final composition after homogenization.

Figure 2a–f shows, respectively, that the clay particles had an average size of 11.36 ( $\mu\text{m}$ ), kaolin particles were 21.28 ( $\mu\text{m}$ ), feldspar particles were 11.52 ( $\mu\text{m}$ ), quartz particles were 13.89 ( $\mu\text{m}$ ), talc particles were 39.66 ( $\mu\text{m}$ ), and the Hap particles were 11.54 ( $\mu\text{m}$ ). Coarser particle size can interfere with the kinetics of sintering reactions, drastically influencing the sintering step of the product. Smaller particle sizes provide more significant surface areas and reactivity between particles, which favor kinetic reactions and the diffusion process during phase transformations [48–50].

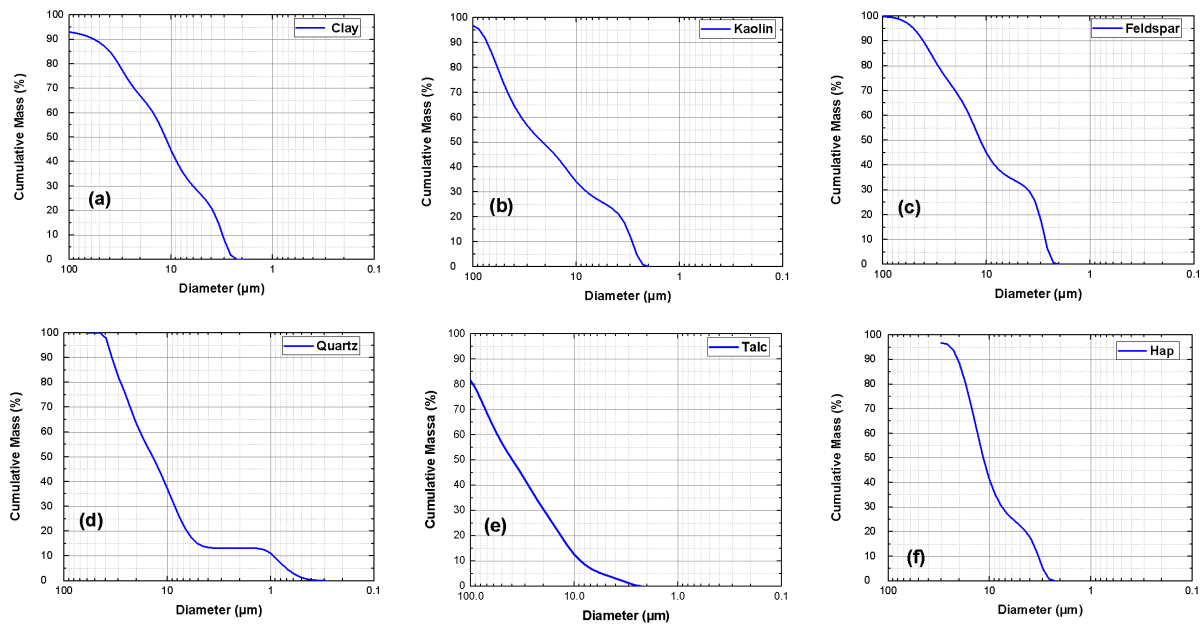


**Figure 2.** Graph of the granulometric distribution of clay (a), kaolin (b), feldspar (c), quartz (d), talc (e), and Hap (f).

Figure 3a–f provides the TG/DTG data for clay, kaolin, feldspar, quartz, talc, and Hap. The TG/DTG curve in Figure 3a obtained from the clay illustrates that the mass loss occurred in two stages. In the first stage, the mass loss was equal to 1.54%, observed at 22 to 200  $^{\circ}\text{C}$ . The origin of the first thermal event was associated with the loss of free and adsorbed water. A mass loss of 12.87% was observed during the second stage (300–800  $^{\circ}\text{C}$ ). This second phase could be attributed to losing organic matter and hydroxyl groups in the clay minerals. The small peaks observed around 800  $^{\circ}\text{C}$  to 1200  $^{\circ}\text{C}$  were due to the transformation of metakaolinite into a spinel-like structure [50]. In Figure 3b, kaolin showed a significant mass loss (15.01%) between 400 and 800  $^{\circ}\text{C}$ , probably associated with the dehydroxylation of kaolinite and mica, transforming it into metakaolinite [51–53]. The total mass losses for clay and kaolin were 15.85% and 16.20%, respectively. Above 900  $^{\circ}\text{C}$ , mullite nucleation occurs with the release of  $\beta$ -quartz from the previously created amorphous structure [54]. In Figure 3c, Feldspar presented a minimum mass loss of 2.24%. In addition, carbonates, sulfates, and organic matter were not found. The important event between 1160 and 1200  $^{\circ}\text{C}$  was probably due to the emergence of the liquid phase of potassium feldspar occurring because of the phase change from microcline to leucite [53–55]. Figure 3d confirms the presence of some characteristic peaks for quartz. The first event characterizes the release of free water between 30 and 100  $^{\circ}\text{C}$  with a mass loss of 0.49%. In the range between 400 and 600  $^{\circ}\text{C}$ , the mass loss of 0.92% was related to the allotropic transformation of  $\alpha$ -quartz to  $\beta$ -quartz. Between 1000 and 1200  $^{\circ}\text{C}$ , the mass loss of 0.14% was associated with quartz crystallization [51]. The total mass loss presented in the test was approximately 2.23%. The talc TG/DTG curve in Figure 3e had a total mass loss of 34.37%. That was mainly related to eliminating  $\text{CO}_2$  from decarbonizing dolomite, which is present in large quantities in the mineral. The mass loss of 27.55% between 700 and 900  $^{\circ}\text{C}$  referred to the release of  $\text{CO}_2$  from the dolomite and dehydroxylation of talc because dolomite is mainly

composed of calcium and magnesium carbonates [55]. In Figure 3f, Hap had a mass loss of 2.41%, associated with free and adsorbed water in the material from 25 to 200 °C. Between 200 °C and 400 °C, a new event occurred with a significant mass loss of 5.31%, probably associated with the loss of hydration water. From 500 °C, the mass suffered small and gradual decreases, with no significant change in the mass. The mass loss above 500 °C was probably due to dehydroxylation. This dehydroxylation occurs because Hap is composed of calcium, phosphate, and hydroxyl ions; the total mass loss was 12.13% [25].

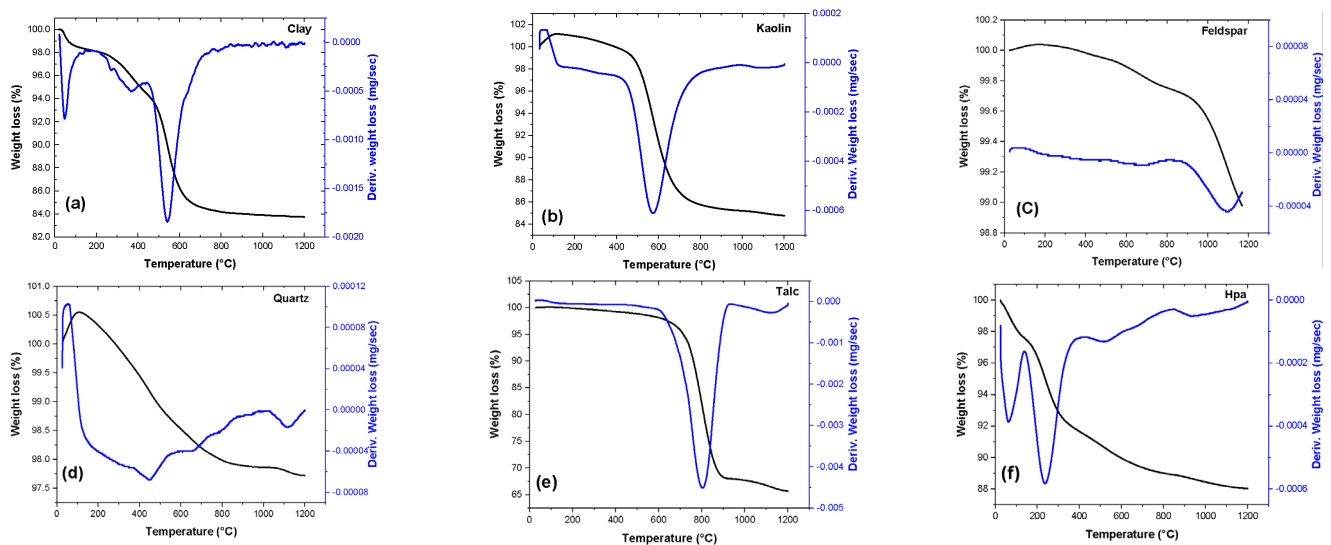


**Figure 3.** Thermogravimetry (TG) and derived thermogravimetry (DTG) curves of clay (a), kaolin (b), feldspar (c), quartz (d), talc (e), and Hap (f). All samples were heated at 5 °C/min.

### 3.2. Mineralogical Phases and Physical–Mechanical Properties of Sintered Samples

As the industry uses production process temperatures between 1190 °C and 1220 °C as a threshold for the production of ceramic tiles, we decided to analyze the temperature of 1200 °C. Therefore, the phase transformations that occurred during the firing cycles were observed.

Figure 4a–d shows the X-ray diffraction patterns of ceramic formulations (standard formulation and formulations with the addition of Hap) sintered at 1200 °C.

Figure 4a identifies the presence of silicon oxide ( $\text{SiO}_2$ ) (JCPDS: 46-1045) and mullite ( $3\text{Al}_2\text{O}_3 \cdot 2\text{SiO}_2$ ) (JCPDS: 15-0776) phases, with the majority phase corresponding to silicon oxide to the detriment of the mullite phase. The emergence of the multitytic phase can be explained by the energetic selection that occurs during the solid phase formation process from the compounds present in the sample. The mullite may have formed due to the preferential reaction between the compounds present. Furthermore, the presence of mullite may have been influenced by the relationship between the levels of elements present in the ceramic tile sample.

In Figure 4b, the following crystalline phases were identified: silicon oxide ( $\text{SiO}_2$ ) (JCPDS: 46-1045), anorthite ( $(\text{Ca}, \text{Na})(\text{Al}, \text{Si})_2\text{Si}_2\text{O}_8$ ) (JCPDS 89-14620), and mullite (JCPDS: 15-0776). The emergence of the anorthite phase may be associated with the addition of Hap in the sample composition, since Hap can transform into anorthite at high temperatures.

In Figure 4c, the crystalline phases of silicon oxide ( $\text{SiO}_2$ ) (JCPDS: 46-1045) and anorthite ( $(\text{Ca}, \text{Na})(\text{Al}, \text{Si})_2\text{Si}_2\text{O}_8$ ) (JCPDS 89-14620) were identified. By increasing the Hap concentration by 5%, in ceramic mass, to 10%, a change in the crystalline phases formed was observed, with a preferential formation of anorthite to the detriment of mullite. This observation suggests the possibility of controlling the formation of crystalline phases in ceramics through the controlled addition of Hap in its composition, a relevant fact for the development of ceramic materials with personalized and tailored properties.



In Figure 4d, the silicon oxide ( $\text{SiO}_2$ ) (JCPDS: 46-1045) and anorthite  $((\text{Ca}, \text{Na})(\text{Al}, \text{Si}_2\text{O}_8))$  (JCPDS 89-14620) phases were identified again. The amount of Hap added did not significantly change the formation of the phases present in the samples.

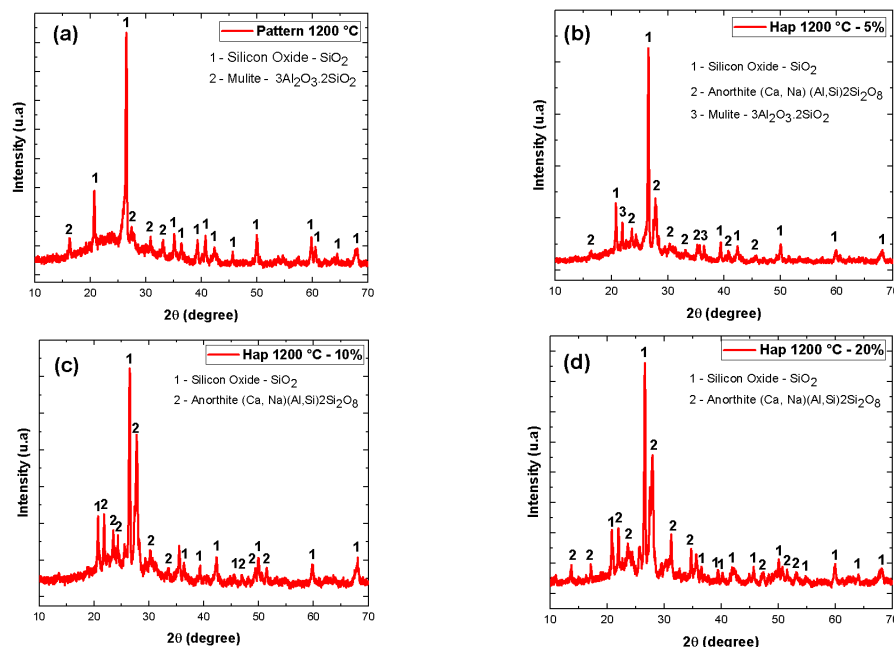


**Figure 4.** XRD patterns of samples (a–d) sintered at 1200 °C.

Anorthite and mullite are desirable in ceramic materials because of their excellent mechanical properties. The increase in temperature led to a decrease in the intensity of the quartz peaks, indicating quartz's partial dissolution and the appearance of mullite and anorthite [51].

Figure 5 shows the impact of sintering temperature (1000 °C, 1100 °C, and 1200 °C) on the physical–mechanical properties (linear shrinkage, apparent porosity, water absorption, and flexural strength) of the standard formulation and the formulations with the addition of Hap (5%, 10%, and 20%).

Figure 5a ( $F_{0a}$ ,  $F_{1a}$ ,  $F_{2a}$ , and  $F_{3a}$ ) show that the linear firing shrinkage increased when the sintering temperature was raised from 1000 °C to 1200 °C. Compared to the standard formulation ( $F_{0a}$ ), formulations added with 5% ( $F_{1a}$ ), 10% ( $F_{2a}$ ), and 20% ( $F_{3a}$ ) Hap exhibited increased linear firing shrinkage of 5% on average, which shows that the Hap, at high temperatures, undergoes greater linear contraction in relation to its initial dimension. Adding Hap to the ceramic tile mass increases the linear shrinkage of the part due to its higher glass transition temperature, as it shrinks more as the temperature increases. In addition, its density helps to reduce the apparent porosity of the ceramic tile, as it fills the spaces between the clay grains and, thus, reduces the number of open pores.

Figure 5b ( $F_{0b}$ ,  $F_{1b}$ ,  $F_{2b}$ , and  $F_{3b}$ ) show that the apparent porosity progressively decreases as the temperature increases from 1000 °C to 1200 °C. When added to the ceramic coating mass, Hap contributes to the reduction in apparent porosity, because hydroxyapatite behaves as a flux, promoting the formation of a denser and more preserved matrix. The presence of Hap promotes the nucleation of the crystals that make up the ceramic mass, leading to a more uniform microstructure and less apparent porosity. The nucleation of Hap in other crystals of the ceramic mass occurs through its interaction of calcium and phosphorus ions as well as its ability to promote the formation of nucleation sites. Furthermore, the presence of Hap acts as a catalyst for the formation of other ceramic phases, such as anorthite and mullite.

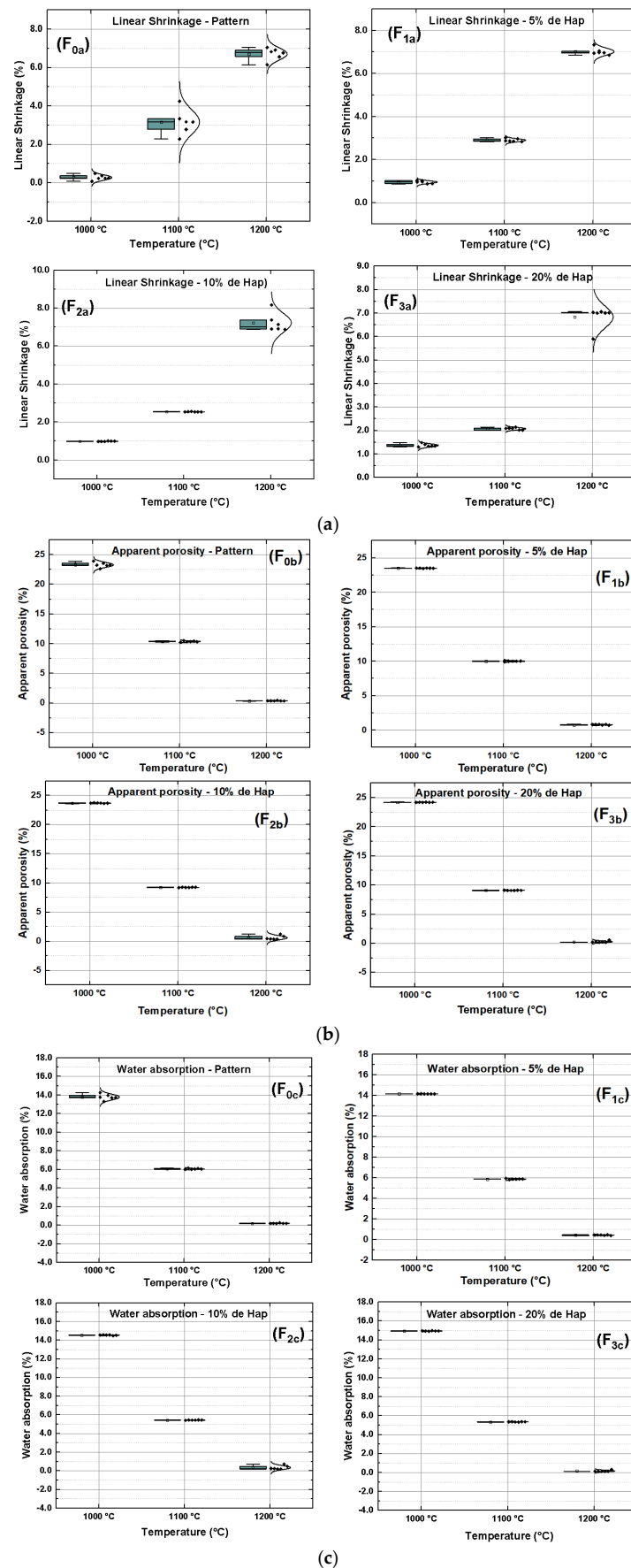
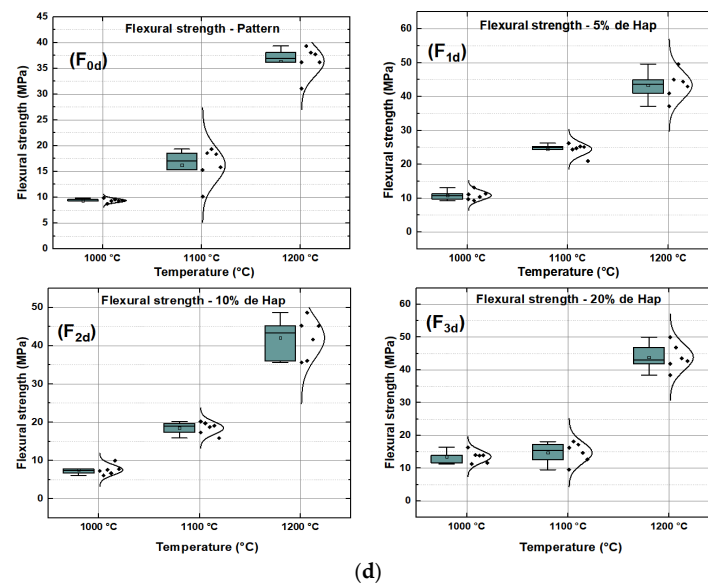


Figure 5. Cont.



**Figure 5.** Dependence of the sintering temperature on the physical–mechanical properties of samples F<sub>0</sub>, F<sub>1</sub>, F<sub>2</sub>, and F<sub>3</sub>. Linear shrinkage (a), apparent porosity (b), water absorption (c), and flexural strength (d).

The decomposition of kaolinite ( $\text{Al}_2\text{Si}_2\text{O}_5(\text{OH})_4$ ), present in both clay and kaolin, generates a large liquid phase formation, helping to reduce the apparent porosity. Other factors that contribute to this phenomenon are potassium ( $\text{K}_2\text{O}$ ) and sodium oxides ( $\text{Na}_2\text{O}$ ), as well as the high alkalinity feldspar, which effectively promotes the liquid phase. This behavior is attributed to the closing of the porosity, which makes the pieces denser, accompanied by shrinkage. The presence of these flux oxides added to the calcium oxide present in the Hap helps increase the degree of sintering and densification due to the greater production of the liquid phase with the increased temperature and expansion of the glass phase [55–57].

Figure 5c (F<sub>0c</sub>, F<sub>1c</sub>, F<sub>2c</sub>, and F<sub>3c</sub>) show that water absorption decreases with increasing temperature from 1000 °C to 1200 °C. The addition of Hap contributed significantly to the decrease in water absorption, as it binds to the surface of the dough particles, promoting the formation of a denser and more resistant matrix as it binds to the surface of the dough particles.

However, there was no significant difference, when considering the cost/benefit, in the addition of Hap from 5% to 10% and from 10% to 20%, because the water absorption decreased in the physical–mechanical properties when the Hap concentration was increased (5%, 10%, and 20%). In general, the addition of Hap promoted a reduction in the water absorption and apparent porosity and a significant increase in the linear shrinkage and mechanical resistance of the ceramic piece, reaching 25% greater than the formulations without Hap.

Figure 5d (F<sub>0d</sub>, F<sub>1d</sub>, F<sub>2d</sub>, and F<sub>3d</sub>) indicate that the mechanical strength progressively increased with the increase in temperature due to the filling of the pores from the melting of flux oxides ( $\text{CaO}$ ,  $\text{K}_2\text{O}$ , and  $\text{Na}_2\text{O}$ ) present in the ceramic mass, leading to increased conditioning due to the formation of an abundant liquid phase, reducing the firing temperature and the porosity of the product. With the addition of Hap, the mechanical resistance increased significantly because the mechanical resistance of the ceramic piece obtained a 15% greater value than the formulation without Hap [58–62].

The results of the mechanical resistance of the porcelain tile ceramic coating with the addition of Hap verify that the formulation with the addition of 5% Hap obtained a resistance of 19.10% greater than the standard formulation. On the other hand, when adding 10% Hap, the resistance increased by only 15.50%, while 20% Hap obtained 20.50% more resistance than the standard formulation. Thus, adding 10% or 20% of Hap would not maximize its use.

Figure 6a–d shows the SEM images acquired from the compositions after sintering at 1200 °C.

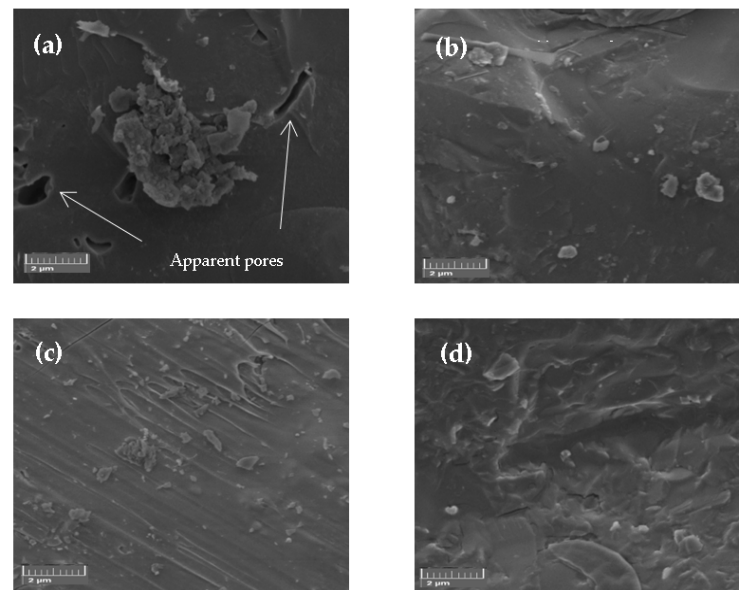


**Figure 6.** SEM images acquired from samples (a–d) sintered at 1200 °C.

Figure 6a illustrates a dense microstructure with few open pores, which is consistent with the observed presence of silicon oxide and mullite phases detected by XRD. These phases are responsible for the high mechanical strength of ceramic materials. Furthermore, the low porosity observed in the image indicates an adequate sintering process, which contributed to the formation of these phases and, consequently, to the good quality of the coating [62]. In Figure 6b, the addition of hydroxyapatite contributed to the absence of pores in the microstructure of the ceramic coating, which is a positive consequence of its high reactivity during the sintering process. Furthermore, the presence of Hap in the formulation facilitated the formation of silicon oxide, anorthite, and mullite phases, responsible for the high mechanical strength. These results suggest that Hap is an excellent option for improving the properties of ceramic tiles. Figure 6c shows the formulation with the addition of 10% Hap, where the formation of silicon oxide and anorthite phases occurred. The absence of pores in both formulations suggests that the presence of Hap facilitates ceramic densification during sintering. However, the amount of Hap added influenced the formation of crystalline phases. Figure 6d shows that the increased Hap content in the ceramic coating mass directly influenced the formation of crystalline phases in the material. The formulations with 5% and 10% Hap added presented differences in the formation of crystalline phases, and the formulation with 10% Hap showed only silicon oxide and anorthite phases. The increase to 20% of Hap led to a significant change in the microstructure and the crystalline phases of the ceramic coating. However, in terms of cost/benefit, the addition of Hap was not considered satisfactory because doubling the amount of Hap in the samples did not significantly increase the mechanical resistance of the sample.

#### 4. Conclusions

The addition of hydroxyapatite (Hap) in ceramic masses has emerged as a sustainable and viable alternative in the production of ceramic tiles with low water absorption, low apparent porosity, and high flexural strength, making them suitable for application in the production of porcelain tiles. The addition of Hap significantly altered the physical–mechanical properties of the sintered samples, particularly the mechanical strength of the ceramic pieces. The incorporation of Hap in the formulations, using 5%, 10%, and 20% by weight, caused significant changes in the physical performance and mechanical

properties of the final product. Compared to the standard formulation, the mechanical resistance increased by more than 15%. Therefore, incorporating Hap in ceramic masses could be a promising technique for the production of ceramic tiles with high mechanical resistance. Even so, further research should be carried out to improve the effectiveness of variations in the amount of Hap added in the crystalline phases and the mechanical strength of ceramic pieces.

**Author Contributions:** Conceptualization: F.P.A. and A.O.L. Data curation: F.P.A., W.M.P.d.A. and R.P.-G. Formal analysis: F.P.A., W.M.P.d.A. and R.P.-G. Investigation: F.P.A. and W.M.P.d.A. Methodology: F.P.A. and W.M.P.d.A. Roles/writing—original draft: F.P.A., W.M.P.d.A., R.P.-G., R.A.L.S. and A.O.L. Writing—review and editing: F.P.A., W.M.P.d.A., R.P.-G., R.A.L.S. and A.O.L. Supervision: R.A.L.S. and A.O.L. Funding acquisition: A.O.L. All authors have read and agreed to the published version of the manuscript.

**Funding:** This research received no external funding.

**Data Availability Statement:** The data presented in this study are available only by the requesting them from the corresponding author due to the further work in progress.

**Conflicts of Interest:** The authors declare no conflict of interest.

## References

1. Silva, J.C.O. Uso de matérias-primas sintéticas em esmaltes cerâmicos industriais: Uma revisão. *J. Ceram. Sci. Technol.* **2020**, *10*, 100–115.
2. Vilarinho, I.S.; Filippi, E.; Seabra, M.P. Development of Eco-Ceramic Wall Tiles with bio-CaCO<sub>3</sub> from Eggshells Waste. *OpenCeram.* **2022**, *9*, 100200. [[CrossRef](#)]
3. De Medeiros, P.S.S.; Lira, H.D.L.; Rodriguez, M.A.; Menezes, R.R.; Neves, G.D.A.; Santana, L.N.D.L. Incorporation of quartzite waste in mixtures used to prepare sanitary ware. *J. Mater. Res. Technol.* **2019**, *8*, 2148–2156. [[CrossRef](#)]
4. Babisk, M.P.; Amaral, L.F.; da Silva Ribeiro, L.; Vieira, C.M.F.; Prado, U.S.; Gadioli, M.C.B.; Oliveira, M.S.; da Luz, F.S.; Monteiro, S.N.; da Costa Garcia Filho, F. Evaluation and application of sintered red mud and its incorporated clay ceramics as materials for building construction. *J. Mater. Res. Technol.* **2020**, *9*, 2186–2195. [[CrossRef](#)]
5. Alekseev, K.; Mymrin, V.; Avanci, M.A.; Klitzke, W.; Magalhães, W.L.E.; Silva, P.R.; Catai, R.E.; Silva, D.A.; Ferraz, F.A. Environmentally clean construction materials from hazardous bauxite waste red mud and spent foundry sand. *Constr. Build. Mater.* **2019**, *229*, 116860. [[CrossRef](#)]
6. da Costa, F.P.; da Silva Morais, C.R.; Pinto, H.C.; Rodrigues, A.M. Microstructure and physico-mechanical properties of Al<sub>2</sub>O<sub>3</sub>-doped sustainable glass-ceramic foams. *Mater. Chem. Phys.* **2020**, *256*, 123612. [[CrossRef](#)]
7. Da Costa, F.P.; da Silva Morais, C.R.; Rodrigues, A.M. Sustainable glass-ceramic foams manufactured from waste glass bottles and bentonite. *Ceram. Int.* **2020**, *46*, 17957–17961. [[CrossRef](#)]
8. Fernandes, J.V.; Guedes, D.G.; da Costa, F.P.; Rodrigues, A.M.; de Araújo Neves, G.; Menezes, R.R.; de Lima Santana, L.N. Sustainable ceramic materials manufactured from ceramic formulations containing quartzite and scheelite tailings. *Sustainability* **2020**, *12*, 9417. [[CrossRef](#)]
9. Uribe, R.; Uvillús, A.; Fernández, L.; Bonilla, O.; Jara, A.; González, G. Deposição Eletroquímica de Hidroxiapatita em Aço Inoxidável Revestido com Tântalo/Nitreto de Tântalo Usando Fluido Corporal Simulado como Meio Eletrolítico. *Coatings* **2022**, *12*, 440. [[CrossRef](#)]
10. Silva, R.H.L.; Neves, G.A.; Ferreira, H.C.; Santana, L.N.L.; Nóbrega, A.C.V.; Menezes, R.R. Use of diopside in ceramic masses for sanitary ware. *Cerâmica* **2019**, *65*, 1–12. [[CrossRef](#)]
11. Da Silva, V.J.; de Almeida, E.P.; Gonçalves, W.P.; da Nóbrega, R.B.; de Araújo Neves, G.; de Lucena Lira, H.; Menezes, R.R.; de Lima Santana, L.N. Mineralogical and dielectric properties of mullite and cordierite ceramics produced using wastes. *Ceram. Int.* **2019**, *45*, 4692–4699. [[CrossRef](#)]
12. Palakurthy, S.; Venu Gopal Reddy, K.; Samudrala, R.K.; Abdul Azeem, P. In vitro bioactivity and degradation behaviour of  $\beta$ -wollastonite derived from natural waste. *Mater. Sci. Eng. C* **2019**, *98*, 109–117. [[CrossRef](#)] [[PubMed](#)]
13. Hossain, S.K.S.; Ranjan, V.; Pyare, R.; Roy, P.K. Study the effect of physicommechanical characteristics of ceramic tiles after addition of river silts and wollastonite derived from wastes. *Construct. Build. Mater.* **2019**, *209*, 315–325. [[CrossRef](#)]
14. Kinnunen, P.; Ismailov, A.; Solismaa, S.; Sreenivasan, H.; Räisänen, M.L.; Levänen, E.; Illikainen, M. Recycling mine tailings in chemically bonded ceramics—A review. *J. Clean. Prod.* **2018**, *174*, 634–649. [[CrossRef](#)]
15. Cengiz, O.; Kara, A. Effect of alkaline-earth oxides on firing behaviour of monoporosa wall tile bodies. *J. Ceram. Process. Res.* **2018**, *19*, 189–197.
16. Lottermoser, B.; Lottermoser, B.G. Introduction to Mine Wastes. In *Mine Wastes*; Springer: Berlin/Heidelberg, Germany, 2010; pp. 1–41.

17. Jones, H.; Boger, D.V. Sustainability and waste management in the resource industries. *Ind. Eng. Chem. Res.* **2012**, *51*, 10057–10065. [[CrossRef](#)]
18. Hughes, D.J.; Shimmield, T.M.; Black, K.D.; Howe, J.A. Ecological impacts of large-scale disposal of mining waste in the deep sea. *Sci. Rep.* **2015**, *5*, 9985. [[CrossRef](#)]
19. Edraki, M.; Baumgartl, T.; Manlapig, E.; Bradshaw, D.; Franks, D.M.; Moran, C.J. Designing mine tailings for better environmental, social and economic outcomes: A review of alternative approaches. *J. Clean. Prod.* **2014**, *84*, 411–420.
20. Adiansyah, J.S.; Rosano, M.; Vink, S.; Keir, G. A framework for a sustainable approach to mine tailings management: Disposal strategies. *J. Clean. Prod.* **2015**, *108*, 1050–1062. [[CrossRef](#)]
21. Zanin, H.; Rosa, C.; Eliaz, N.; Maio, P.; Marciano, F.; Lobo, A. Deposição assistida de nano-hidroxiapatita em andaimes de óxido de nanotubos de carbono esfoliados. *Nanoscale* **2015**, *7*, 10218–10232. [[CrossRef](#)]
22. Grinet, M.A.; Zanin, H.; Granato, A.E.C.; Porcionatto, M.; Marciano, F.R.; Lobo, A.O. Preparação rápida de scaffolds de nanotubos de carbono alinhados verticalmente com nanohidroxiapatita. *J. Mater. Química B* **2014**, *2*, 1196–1204. [[CrossRef](#)]
23. Rodrigues, B.V.; Leite, N.C.; das Neves Cavalcanti, B.; da Silva, N.S.; Marciano, F.R.; Corat, E.J.; Webster, T.J.; Lobo, A.O. Óxido de grafeno/nanotubos de carbono de paredes múltiplas como scaffolds nanofeatured para a deposição assistida de nanohidroxiapatita: Caracterização e avaliação biológica. *Int. J. Nanome.* **2016**, *11*, 2569.
24. Nardecchia, S.; Carriazo, D.; Ferrer, M.L.; Gutierrez, M.C.; del Monte, F. Arquiteturas macroporosas tridimensionais e aerogéis construídos com nanotubos de carbono e/ou grafeno: Síntese e aplicações. *Química Soc. Rev.* **2013**, *42*, 794–830. [[CrossRef](#)]
25. Barbosa, M.C.R.; Messmer, N.R.; Brazil, T.R.; Marciano, F.; Lobo, A.O. The effect of ultrasonic irradiation on the crystallinity of nano-hydroxyapatite produced via the wet chemical method. *Mater. Sci. Eng. C* **2013**, *33*, 2020–2625. [[CrossRef](#)] [[PubMed](#)]
26. Biffi, G.O. *Grês Porcelanato: Manual de Fabricação e Técnicas de Emprego*; Gruppo Editoriale: São Paulo, Brazil, 2006.
27. Barba, A. *Materias Primas Para la Fabricación de Soportes de Baldosas Cerámicas*; Instituto de Tecnología Cerámica: São Paulo, Brazil, 1997.
28. ABNT NBR 15270:2017; Componentes Cerâmicos—Blocos e Tijolos Para Alvenaria: Métodos de Ensaio. Associação Brasileira de Normas e Técnicas: São Paulo, Brazil, 2017.
29. NBR 13816; Associação Brasileira de Normas Técnicas. Placas Cerâmicas Para Revestimento: Terminologia. Associação Brasileira de Normas Técnicas: São Paulo, Brazil, 1997.
30. NBR 13818; Associação Brasileira de Normas Técnicas. Placas Cerâmicas PARA Revestimento—Especificações e Métodos de Ensaio. Associação Brasileira de Normas Técnicas: São Paulo, Brazil, 1997.
31. NBR 15463; Associação Brasileira de Normas Técnicas. Placas Cerâmicas Para Revestimento—Porcelanato. Associação Brasileira de Normas Técnicas: São Paulo, Brazil, 2013.
32. NBR 7181; Associação Brasileira de Normas Técnicas-Abnt. Solo—Análise Granulométrica. Associação Brasileira de Normas Técnicas: São Paulo, Brazil, 2017.
33. ASTM D790; American Society for Testing and Materials. Standard Test Methods for Flexural Properties of Unreinforced and Reinforced Plastics and Electrical Insulating Materials. Associação Brasileira de Normas Técnicas: São Paulo, Brazil, 2002.
34. ISO 13006:2019; ABNT. Placas Cerâmicas—Definições, Classificações, Características e Marcação. ABNT: Rio de Janeiro, Brazil, 2019.
35. Mahmoudi, S.; Bennour, A.; Meguebli, A.; Srasra, E.; Zargouni, F. Characterization and traditional ceramic application of clays from the Douiret region in South Tunisia. *Appl. Clay Sci.* **2016**, *127–128*, 78–87. [[CrossRef](#)]
36. De Aza, A.H.; Turrillas, X.; Rodriguez, M.A.; Duran, T.; Pena, P. Time-resolved powder neutron diffraction study of the phase transformation sequence of kaolinite to Mullite. *J. Eur. Ceram. Soc.* **2014**, *34*, 1409–1421. [[CrossRef](#)]
37. Menezes, R.R.; de A Neves, G.; Ferreira, H.C. State of the art about the use of wastes as alternative to ceramic raw materials. *Rev. Bras. De Eng. Agrícola E Ambient.* **2002**, *6*, 303–313. [[CrossRef](#)]
38. Chen, C.Y.; Tuan, W.H. The processing of kaolin powder compact. *Ceram. Int.* **2001**, *27*, 795–800. [[CrossRef](#)]
39. Brindley, G.W.; Nakahira, M. The kaolinite-mullite reaction series: I, a survey of outstanding problems. *J. Am. Ceram. Soc.* **1959**, *42*, 311–314. [[CrossRef](#)]
40. McConville, C.J.; Lee, W.E. Microstructural evolution in fired kaolinite. *Brit. Ceram. Trans.* **1998**, *97*, 162–168.
41. Soares, R.A.L. *Efeitos da Adição de Carbonatos em Formulações de Massa Para Revestimento Cerâmico Utilizando Matérias-Primas do Piauí*; Tese de Doutorado—Universidade Federal do Rio Grande do Norte: Natal, Brazil, 2010.
42. Chen, C.Y.; Lan, G.S.; Tuan, W.H. Microstructural evolution of Mullite during the sintering of kaolin powder compact. *Ceram. Int.* **2000**, *26*, 715–720. [[CrossRef](#)]
43. Özkan, İ. Ceramic properties of a Turkish clay in the Aydın region. *J. Ceram. Proc. Res.* **2014**, *15*, 44–47.
44. Issaoui, M.; Limousy, L.; Lebeau, B.; Bouaziz, J.; Fourati, M. Design and characterization of flat membrane supports elaborated from kaolin and aluminum powders. *Comptes Rendus Chim.* **2016**, *19*, 496–504. [[CrossRef](#)]
45. Santos, P.S. *Ciência e Tecnologia de Argilas*, 2nd ed.; Edgard Blücher: São Paulo, Brazil, 1989.
46. Liu, D.M.; Troczynski, T.; Tseng, W.J. Water-based sol-gel synthesis of hydroxyapatite: Process development. *Biomaterials* **2001**, *22*, 1721. [[PubMed](#)]
47. Nour, W.; Mostafa, A.; Ibrahim, D. Recycled wastes as precursor for synthesizing wollastonite. *Ceram. Int.* **2008**, *34*, 101–105. [[CrossRef](#)]

48. Chin, C.L.; Ahmad, Z.A.; Sow, S.S. Relationship between the thermal behaviour of the clays and their mineralogical and chemical composition: Example of Ipoh, Kuala Rompin and Mersing (Malaysia). *Appl. Clay Sci.* **2017**, *143*, 327–335. [[CrossRef](#)]
49. JFigueiredo, M.R.; Fernandes, I.M.M.; Silva, V.J.; Neves, G.A.; Ferreira, H.C.; Santana, L.N.L. Influence of composition and processing variables of clay-based formulations—Use in refractory materials. *Ceramica* **2018**, *64*, 10–19.
50. Ismail, H.; Shamsudin, R.; Hamid, M.A.A. Effect of autoclaving and sintering on the formation of  $\beta$ -wollastonite. *Mater. Sci. Eng. C* **2016**, *58*, 1077–1081. [[CrossRef](#)]
51. Mendonça, A.M.G.D.; Cartaxo, J.M.; Menezes, R.R.; Santana, L.N.L.; Neves, G.A.; Ferreira, H.C. Moisture expansion of ceramic tiles produced using kaolin and granite wastes. *Ceramica* **2012**, *58*, 216–224. [[CrossRef](#)]
52. Ozturk, Z.B. Effect of addition of Avanos's (Nevsehir) clays on the physical and microstructure properties of ceramic tile. *J. Aust. Ceram. Soc.* **2016**, *53*, 101–107. [[CrossRef](#)]
53. Marino, L.F.B.; Boschi, A.O. A Expansão Térmica dos Revestimentos Cerâmicos. Parte VI: Comparação Entre os Efeitos das Adições de Calcita, Dolomita e Talco. *Ceram. Ind.* **2000**, *5*, 21–23.
54. Teixeira, S.R.; Souza, A.E.; Carvalho, C.L.; Reynoso, V.C.S.; Romero, M.; Rincon, J.M. Characterization of a wollastonite glass-ceramic material prepared using sugar cane bagasse ash (SCBA) as one of the raw materials. *Mater. Char.* **2014**, *98*, 209–214. [[CrossRef](#)]
55. Varela, M.L.; Formiga, F.L.; Dutra, R.P.S.; Nascimento, R.M.D.; Paskocimas, C.A. Influence of kaolin waste addition on technological properties of a standard stoneware formulation produced in industrial scale. *Ceramica* **2009**, *55*, 209–215. [[CrossRef](#)]
56. Moulton, B.J.A.; Rodrigues, A.M.; Pizani, P.S.; Sampaio, D.V.; Zanotto, E.D. A Raman investigation of the structural evolution of supercooled liquid barium disilicate during crystallization. *Int. J. Appl. Glas. Sci.* **2018**, *9*, 510–517. [[CrossRef](#)]
57. Rodrigues, A.M.; Silva, L.D.; Zhang, R.; Soares, V.O. Structural effects on glass stability and crystallization. *Crystengcomm* **2018**, *20*, 2278–2283. [[CrossRef](#)]
58. Moulton, B.J.A.; Rodrigues, A.M.; Sampaio, D.V.; Silva, L.D.; Cunha, T.R.; Zanotto, E.D.; Pizani, P.S. The origin of the unusual DSC peaks of supercooled barium disilicate liquid. *Crystengcomm* **2019**, *21*, 2768–2778. [[CrossRef](#)]
59. Silva, D.; Sampaio, D.; Silva, J.; Rodrigues, A.; Pena, R.; Moulton, B.; Pizani, P.; Rino, J.; Silva, R. Synthesis of PbO-SiO<sub>2</sub> glass by CO<sub>2</sub> laser melting method. *J. Non-Cryst. Solids* **2019**, *522*, 119572. [[CrossRef](#)]
60. Ozturk, Z.B. Microstructural characterization of Mullite and anorthite-based Porcelain tile using regional clay. *J. Ceram. Process. Res.* **2016**, *17*, 555–559.
61. Fernández-Pradas, J.; Serra, P.; Morenza, J.; De Aza, P. Pulsed laser deposition of pseudowollastonite coatings. *Biomaterials* **2002**, *23*, 2057–2061. [[CrossRef](#)]
62. Wenk, H.-R. Polymorphism of wollastonite. *Contrib. Miner. Pet.* **1969**, *22*, 238–247. [[CrossRef](#)]

**Disclaimer/Publisher's Note:** The statements, opinions and data contained in all publications are solely those of the individual author(s) and contributor(s) and not of MDPI and/or the editor(s). MDPI and/or the editor(s) disclaim responsibility for any injury to people or property resulting from any ideas, methods, instructions or products referred to in the content.